Maximum Power Point Tracking for photovoltaic system applied to DC/DC/AC inverter based on Modular Multi-level Converter structure

TRAN HUNG CUONG [1], AN THI HOAI THU ANH [2✉]

[1]*Faculty of Electrical and Electronic Engineering, Thuyloi University*
Vietnam

[2]*Department of Electrical Engineering, University of Transport and Communications*
Vietnam

e-mail: htanh.ktd@utc.edu.vn

Abstract: Nowadays, solar power is a potential alternative energy source. To get the best maximum power from solar power, it is necessary to have a strong enough inverter structure and a good control algorithm. This paper presents the Maximum Power Point Tracking (MPPT) algorithm of a solar PV system applied to a DC/DC/AC inverter to obtain maximum power, in which the DC/DC rectifier uses a Boost Converter and the DC/AC inverter uses a Modular Multilevel Converter (MMC). The purpose is to convert electricity from the grid-connected PV system. The MPPT algorithm uses the Incremental Conductance – Integral Regulator (INC-IR) method to find the maximum power point quickly and accurately in different weather conditions. The operation of an MMC uses the Nearest Level Modulation (NLM) method combined with a capacitor voltage balance algorithm to generate maximum AC voltage levels and control the capacitor voltage balance in the MMC. The Nearest Level Modulation method has the advantage of providing a very low valve switching frequency to increase the lifetime of the semiconductor valve. A closed-loop circuit with the PI controller performs the grid-connected power control process. This control and modulation process will produce sinusoidal alternating current (AC) and voltage with a sound total harmonic distortion (THD) index. The simulation of the system will be performed on MATLAB/Simulink software to demonstrate the performance of the proposed method and applied to a 21-level MMC.

Key words: Boost Converter, grid-connected, Maximum Power Point Tracking, Modular Multilevel Converter, solar energy

1. Introduction

Nowadays, solar power has contributed a large amount of power to supply loads. To connect solar power to the grid smoothly, valuable solutions for inverters and control algorithms for inverters are needed. Therefore, research on inverter control applied to grid-connected solar power is receiving considerable attention [1]. Grid-connected PV systems do not require storage systems because they operate in parallel with the grid [2, 3]. DC/AC converters usually enable the grid connection of PV systems. Many studies have been conducted on inverters to convert DC/AC power to PV systems [4], as well as traditional inverters such as voltage source inverters (VSIs) and current source inverters (CSIs). The output from VSI and CSI consists of only two voltage levels. They have a structure with a small number of components and simple control. Still, the switching loss is often large, and the voltage change rate is significant, so when designing, it is necessary to use additional filters with large sizes, which are frequently used for applications with low voltage ranges [5, 6]. However, when a large-capacity PV system needs to be connected to a medium-voltage or high-voltage grid, the application of the above converters faces many limitations [7]. To overcome these limitations, multi-level converters for grid-connected PV systems are necessary, including cascaded H-bridge (CHB), neutral-point-clamped (NPC) converters and an MMC [8–10]. An MMC has outstanding advantages for application to high voltage conversion systems among these converters. Specifically, it can create an unlimited number of levels to divide the value of the levels to ensure that the semiconductor valves do not have to withstand voltages exceeding their rated tolerance [11]. It is easy to apply the NLM method and the capacitor voltage balancing an algorithm with a very low valve switching frequency that other modulation methods cannot perform [12]. The disadvantage of an MMC is the existence of a circulating current in the circuit, which causes power loss and increases the tolerance limit of semiconductor components. When the number of levels is large, the MMC control process becomes complicated [13]. When an MMC connects the PV system to the grid, the problem that needs to be solved is to ensure optimal absorption of solar energy while ensuring that the MMC operates to meet technical requirements such as: balancing the voltage of the capacitors in each phase, the ACs and voltages must be sinusoidal and meet the THD index well. This paper will present the MPPT algorithm applied to the conversion system, including the DC/DC converter based on a Boost Converter and the DC/AC inverter using an MMC. The combination of these two converters has a specific purpose: Boost Converter increases the voltage to the input DC voltage value of the MMC and, at the same time, has the function of controlling the maximum power capacity of the PV system based on the INC-IR and MPPT algorithms. The MMC operates to create AC and voltage with good quality to connect to the AC grid. This aims to determine the maximum power point as quickly and accurately as possible by opening and closing semiconductor valves to improve the operating efficiency and performance of the PV source. The MPPT method is widely used in stand-alone PV systems and grid-connected PV systems and is used when the solar radiation is unstable [14]. In this paper, the MPPT algorithm is applied to the Boost Converter to generate a semiconductor valve switching signal to change the operating voltage of the solar cell while increasing the DC voltage supplied to the inverter. To solve these problems, the paper proposes the algorithm INC−IR method, which automatically detects MPPT points to optimise solar energy sources for the system to achieve maximum power. In addition, the Capacitor Voltage Balancing method, the NLM method combined with the PI controller in the current and voltage regulation loop will be applied

to ensure the balance of capacitor voltage in the MMC while creating current and voltage on the AC side of the MMC in the form of a sinusoid with a small THD index. The simulation and verification of the system operation are performed on MATLAB/Simulink software. The results have shown the effectiveness of the proposed method and can be applied to PV systems in practice.

2. PV working characteristics and MPPT algorithm

2.1. Model and working characteristics of PV

PV systems receive energy from the sun, so their capacity depends heavily on weather conditions. In addition, the way the equipment is installed, the arrangement, dust, etc., can all affect the operation of PV [15]. This article only considers two main factors affecting the PV system: temperature (°C) and radiation intensity (W/m^2). The parameters of a solar cell under standard conditions (a radiation intensity of 1000 W/m^2, temperature 25°C) are presented in Table 1.

Table 1. Parameters of a PV cell SPR-305E-WHT-D

Parameter	Symbol	Value
Capacity max	P_{max}	305 W
Voltage at maximum point MPP	V_{MPP}	54.7 V
Current at maximum point MPP	I_{MPP}	5.58 A
Open circuit voltage	V_{OC}	64.2 V
Short circuit current	I_{SC}	5.96 A

The nature of PV panels is to act as current sources, receiving energy from the sun and emitting current with working characteristics, as shown in Fig. 1(a). This paper investigates a PV system with 5 PV strings connected in series ($N_s = 5$); each PV string consists of 66 PV cells connected in parallel ($N_p = 66$). The total PV system capacity is $P_{MMP} = 305.5.66 = 100$ (kW). The maximum voltage value $V_{MMP} = 54.7.5 = 273$ (V). The maximum current value $I_{MMP} = 5.58.66 = 368.28$ (A). The ideal PV model described in Fig. 1(b) is a model that does not consider the effects of R_s and R_{sh}, ($R_s = 0$ và $R_{sh} = \infty$).
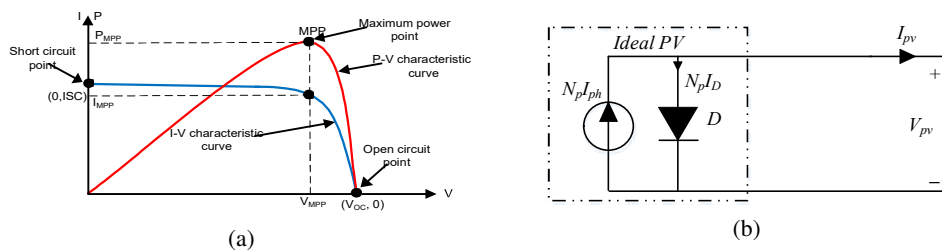

Fig. 1. P–V and I–V characteristics of PV (a); equivalent diagram of ideal PV (b)

The I–V characteristic equation obtained for PV when ignoring R_s and R_{sh} is as in Eq. (1).

$$I_{pv} = N_p I_{ph} - N_p I_D = N_p I_{ph} - N_p I_s (e^{\frac{qV_d}{N_s(nKT)}} - 1). \tag{1}$$

$N_p I_{ph}$ is a constant current source corresponding to certain weather conditions, and $N_p I_D$ is the diode's I–V characteristic, a monotonic curve in the positive VD voltage range. From there, according to Eq. (1), we can represent the relationship between current – voltage and power – voltage (I–V and P–V characteristics) of the SPR-305E-WHT-D solar panel under standard conditions, as shown in Fig. 3 [16].

From Fig. 2, it can be seen that the I–V and P–V relationships are nonlinear. The characteristic curves are not permanently fixed but are greatly influenced by weather factors (temperature, radiation). Under standard STC conditions, the solar cell under consideration can provide a maximum power of 100 kW with an open circuit voltage $V_{OC} = 321$ V and a short circuit current $I_{SC} = 393.36$ A. From the characteristic curve in Fig. 2, we can see that the output power of the solar cell is an adjustable quantity depending on the solar cell's voltage. We always want the output power to reach the highest level to maximise energy use. The point where the solar cell operates at the highest capacity is called the maximum power point (MPP).
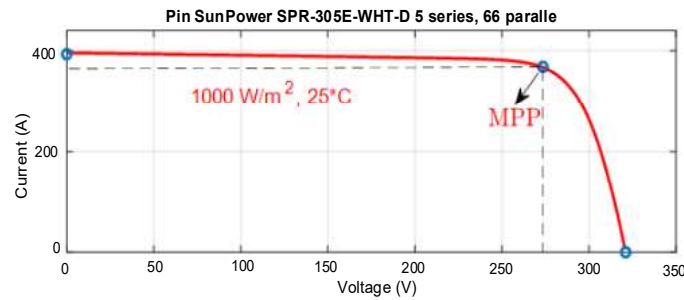
(a) Solar cell characteristics SPR-305E-WHT-D (5 series, 66 parallel)
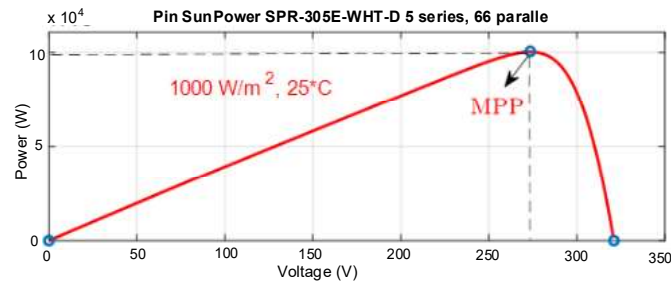
(b)

Fig. 2. Solar cell characteristics SPR-305E-WHT-D (5 series, 66 parallel)

Figure 3 describes the change in the I–V and P–V characteristics of the cell when the solar radiation intensity changes [16]. From Fig. 3, it can be seen that when changing the condition of solar radiation intensity from $W = 250$ W/m^2 to $W = 500$ W/m^2 and $W = 1000$ W/m^2, the current

and power values of the I–V and P–V characteristics change, but the shape of the curve does not change. Figure 4 describes the change of the I–V characteristic curve and P–V characteristic curve of the battery when the temperature changes from 15° to 25° and 50°.


(a)

(b)
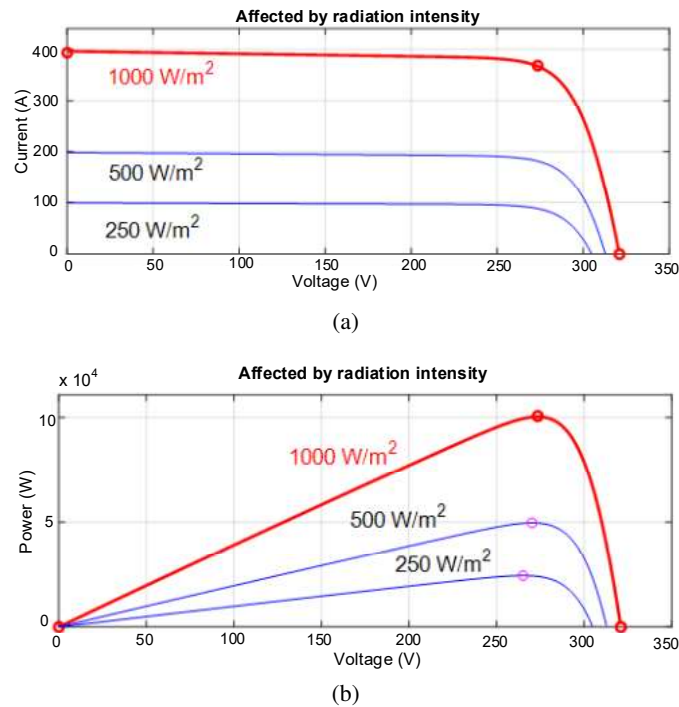
Fig. 3. Effect of radiation intensity on solar cell characteristics


(a)

(b)
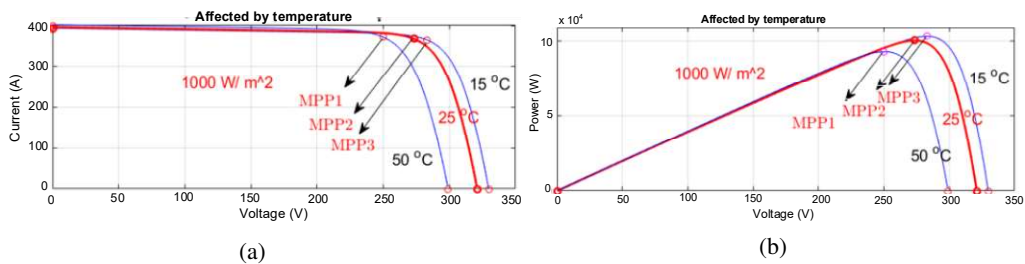
Fig. 4. Effect of temperature on solar cell characteristics

From the above surveys, it can be concluded that when the radiation intensity or environmental temperature changes, the point with the highest power also moves, and the location of that MPP cannot be known in advance. Therefore, an algorithm must be developed to track the movement of the MPP. From there, the solar power system must be imposed to operate at the found MPP.

2.2. Method to detect MPPT point in Boost Converter

The Boost Converter increases the V_{dc} voltage from the solar cell to achieve a higher value for the MMC input. Thanks to the MPPT algorithm, the Boost Converter also plays a vital role in helping the PV operate at its maximum power point. Figure 5 shows the general structure of the MPPT controller for the Boost Converter when coupled with the PV system to the grid.
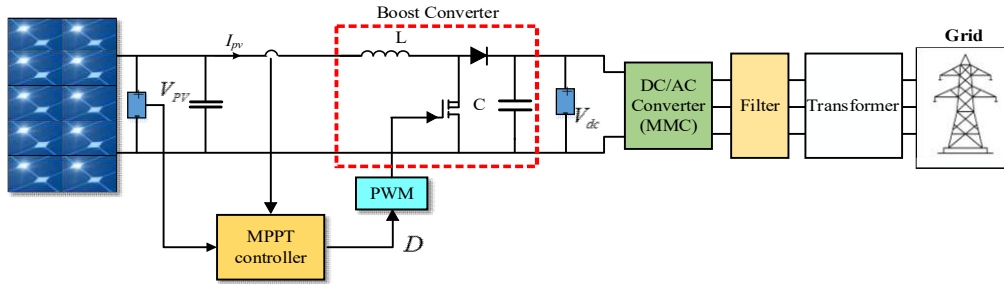

Fig. 5. MPPT algorithm structure diagram using Boost Converter

The Boost Converter generates an output voltage greater than an input voltage; the voltage and current relationship between output and input are described in Eqs. (2) and (3).

$$\frac{V_{\text{out}}}{V_{\text{in}}} = \frac{V_{dc}}{V_{pv}} = \frac{1}{1-D}, \tag{2}$$

$$\frac{I_{\text{out}}}{I_{\text{in}}} = \frac{I_{dc}}{I_{pv}} = 1-D. \tag{3}$$

V_{dc} is the output voltage of the Boost Converter, V_{pv} is the operating voltage of the PV, and D is the modulation ratio of the Boost Converter. For the PV to operate according to the maximum power point, we can adjust the voltage of the solar cell V_{pv} to reach the V_{MMP} value by adjusting the D factor of the Boost Converter. Figure 5 shows that the MPPT algorithm receives information about the voltage and current at which the PV operates. From there, the algorithm evaluates the operating status of the PV to reach its maximum capacity.

If this has not been achieved, the algorithm will adjust the D coefficient of the Boost Converter to increase or decrease accordingly. Specifically, consider the two times k and $k-1$ in Fig. 6; voltage and power at two times are $V_{(k)}$, $V_{(k-1)}$ và $P_{(k)}$, $P_{(k-1)}$.

If $\Delta P = P_{(k)} - P_{(k-1)} > 0$, $\Delta V = V_{(k)} - V_{(k-1)} > 0$, the system works in direction 1.

If $\Delta P = P_{(k)} - P_{(k-1)} < 0$, $\Delta V = V_{(k)} - V_{(k-1)} < 0$, the system works in direction 2.

If $\Delta P = P_{(k)} - P_{(k-1)} > 0$, $\Delta V = V_{(k)} - V_{(k-1)} < 0$, the system works in direction 3.

If $\Delta P = P_{(k)} - P_{(k-1)} < 0$, $\Delta V = V_{(k)} - V_{(k-1)} > 0$, the system works in direction 4.

If $\Delta P = P_{(k)} - P_{(k-1)} = 0$, $\Delta V = V_{(k)} - V_{(k-1)} = 0$, the system works at the MPP.

Based on the P–V characteristic curve, if we want to increase the PV operating point to its maximum, we need to change the voltage V_{pv} by the voltage V_{MPP}; then the PV capacity is adjusted to P_{MMP}. From the formula $V_{pv} = V_{dc}/(1-D)$ of the Boost Converter, we keep V_{dc} fixed; if we want to change V_{pv}, we need to change the coefficient D, thereby making the solar panel system operate at the desired characteristic point. When keeping V_{dc} fixed:

Increase D: $D(k) = D(k-1) + \Delta D \rightarrow$ Reduce V_{pv};
Reduce D:$D(k) = D(k-1) - \Delta D \rightarrow$ Increase V_{pv}.
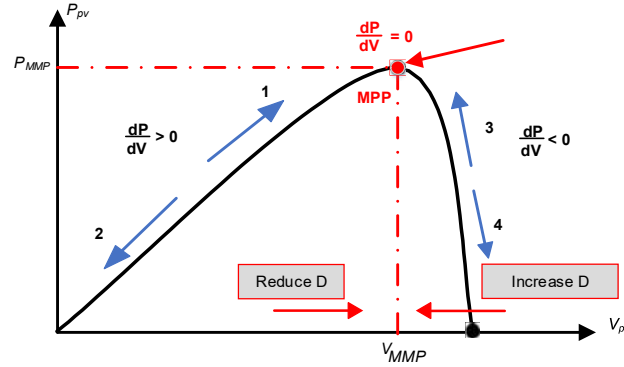
Fig. 6. PV working states

The value of $D(k)$ is updated continuously after each change. The increase or decrease of D previously depends on the choice of the step of changing ΔD of each cycle. ΔD is the step of changing the D of the algorithm; determining ΔD is very important. The first method is to give ΔD a fixed value; the algorithm will perform the maximum power point detection by changing D step by step (each step only changes a fixed amount of ΔD). If ΔD is chosen too small, the algorithm can find the MMP accurately, but tracking the maximum power point will take a long time. When the radiation or temperature changes suddenly, the algorithm becomes less effective. If ΔD is chosen to be significant, the algorithm will track faster, but because of the significant step size, the algorithm is prone to large fluctuations, and it isn't easy to find the exact MPP.

2.3. INC-IR method automatically detects MPPT points

The INC-IR (Incremental Conductance – Integral Regulator) method is proposed as an effective way to adjust the D coefficient [17]. There is no need to depend on a fixed ΔD. This method calculates the ΔD value that needs to be changed based on the slope of the power curve. We can express the relationship between the change in power and voltage as Eq. (4).

$$\frac{\mathrm{d}P}{\mathrm{d}V} = \frac{\mathrm{d}(VI)}{\mathrm{d}V} = I + V\frac{\mathrm{d}I}{\mathrm{d}V} \leftrightarrow \frac{I}{V} + \frac{\mathrm{d}I}{\mathrm{d}V} = e. \tag{4}$$

Let e be the slope of the power and voltage curve. ΔD is no longer kept constant but changes continuously based on the power change. If the power change is small, ΔD is adjusted to increase to reduce the algorithm execution time. If the power change is small, ΔD is decreased to find the exact MPP. The IC method is combined with an integration step to adjust ΔD according to the power change [18]. The algorithm flowchart is shown in Fig. 7.

Specifically, the algorithm: Initially, the D value is fixed at D_0, but when starting the MPPT algorithm, the voltage and current values are saved in the memory area. Based on the voltage change, the current slope e is calculated according to the equation $\Delta D = K.\int e$ (K is chosen to be
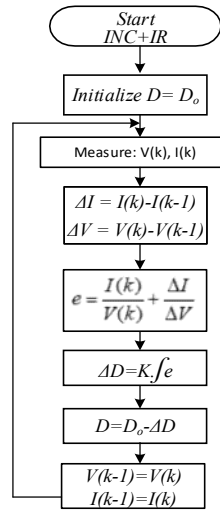
Fig. 7. Flowchart of the INC+IR method algorithm

5 to 7 according to [19]). The new D value is calculated by $D_o - \Delta D$. Thanks to this method, the slope e is adjusted to 0 (at this time, the system works at the MPP). The INC+IR method helps the PV system follow the maximum power point faster and more accurately than conventional methods. At the end of each change cycle, the voltage and current $V(k)$, $I(k)$ are updated to the controller. The MPPT algorithm always ensures that the PV operates in the desired state.

3. MMC structure and NLM modulation method

3.1. MMC converter structure

The MMC structure consists of three phases, as shown in Fig. 8; each phase comprises two valve branches, including the upper and lower branches, and each branch contains the number N of Submodules (N SMs) (total SMs on phase 1 is $2N$). On each branch, an additional L_o inductor and R_o resistor are connected. The AC voltage on each phase is taken at the midpoint between the two inductors of each branch. L_o limits the short-circuit current from outside into the MMC and helps the capacitors to charge better and smooth the output voltage wave; R_o represents the losses in the SMs [20]. The input DC voltage is supplied by a common source V_{dc}. At each time, on a phase, there are always N SMs inserted to create a step voltage level of $2N + 1$ according to the NLM algorithm, and then each SM will be subjected to a voltage level of V_{dc}/N. Each SM is a half-bridge inverter connected in parallel with the capacitor, with the working principle shown in Fig. 9.

Figure 9 describes each SM's on-off state of valves S1 and S2. The current direction is conventionally positive with Figs. 9(a) and (b) and negative with Figs. 9(c) and (d). The on-off states are described explicitly in Table 2.

Since the three phases of the MMC have the same structure when calculating, one phase will be modelled; the remaining phases can be done similarly. From Fig. 10, the output voltage of the

MMC is written as (5).

$$e_v = \frac{v_L - v_U}{2} = \frac{v_L + v_U}{2} - v_U = \frac{V_{dc}}{2} - v_U = \frac{-V_{dc}}{2} + v_L. \tag{5}$$
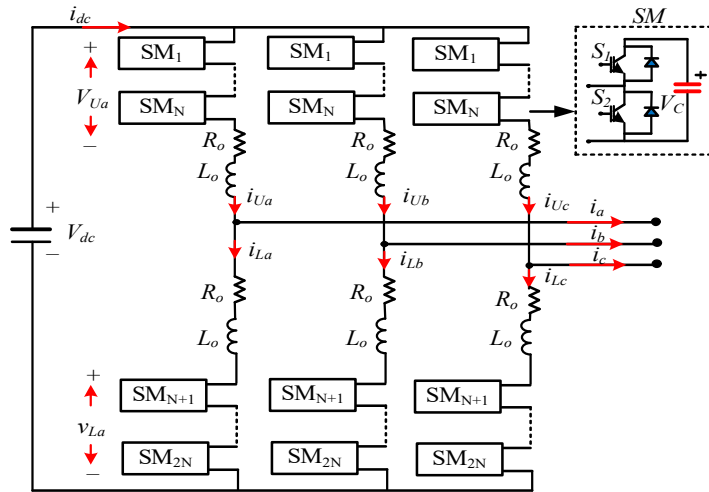

Fig. 8. MMC structure
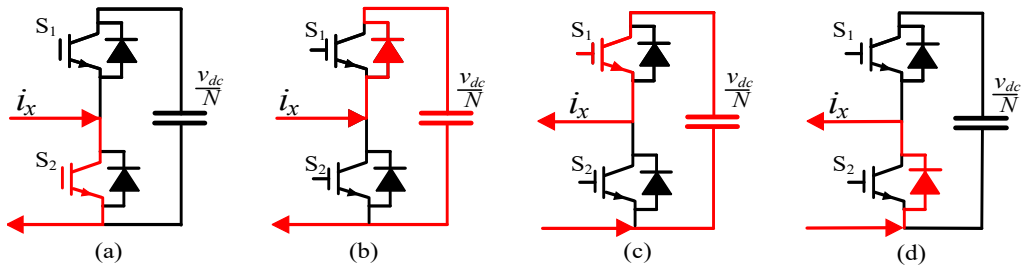
Fig. 9. Switching states of each SM

Table 2. Working status of SM

Valve status		Output voltage	Direction of current	Capacitor state
S_1	S_2			
1	0	V_{dc}/N	+	Charge
0	1	0	+	Shortcut
1	0	V_{dc}/N	−	Discharge
0	1	0	−	Shortcut
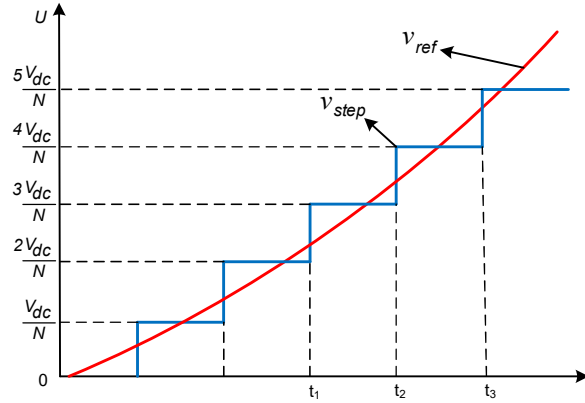
Fig. 10. Reference voltage and modulation voltage of NLM method

According to the document [18], the reference value for the AC electromotive force of the MMC is as (6).

$$e_v^{\text{ref}} = \frac{m.V_{\text{dc}}}{2} \cos \omega t = u_L - u_U. \tag{6}$$

From (5) and (6), the modulating signal for v_U^{ref}, v_L^{ref}, is written as (7).

$$\begin{cases} v_U^{\text{ref}} = \dfrac{V_{\text{dc}}}{2} - e_v^{\text{ref}} = \dfrac{V_{\text{dc}}}{2}(1 - m \cos \omega t) \\ v_L^{\text{ref}} = \dfrac{V_{\text{dc}}}{2} + e_v^{\text{ref}} = \dfrac{V_{\text{dc}}}{2}(1 + m \cos \omega t) \end{cases}. \tag{7}$$

From Eq. (6), the modulation process for the MMC must produce the voltages of the upper and lower branches of the MMC, which are v_U and v_L, respectively. The amount set for v_L^{ref}, v_U^{ref} is calculated from Formula (7). This paper will focus on the NLM method because of its advantages, such as expanding many SMs in large numbers and switching with small losses.

3.2. NLM method for MMC

The principle of the NLM method applied to the MMC is based on dividing the DC voltage equally among the SMs and arranging these voltages to follow the desired reference voltage. Then, the total voltage of the SMs is in a ladder form following the desired reference voltage. Figure 10 describes the form of the reference voltage and the modulation voltage (ladder form) according to the NLM method. The task of the NLM algorithm in the MMC is to find the number of SMs that need to be inserted at each time t_1, t_2, t_3, through rounding calculation.

There, v_{ref} is the desired reference voltage, and v_{step} is the step voltage according to the NLM method. Figure 10 shows that the v_{step} output voltage combines many step voltage levels, following the desired v_{ref} voltage line. If the number of voltage levels increases, the output voltage quality will be higher, and the harmonic distortion will decrease. Ideally, when the V_{dc} value remains constant, if the number of step voltages increases, the output voltage will have a form almost

identical to the reference voltage. This is very important for improving and enhancing voltage quality. When applying the NLM method to the MMC, we will divide the upper and lower branch voltages equally for the SMs on each branch. The magnitude of a step voltage level is equal to the voltage on an SM. If we ignore the voltage on the bypass mode SMs, the relationship between the voltage on each SM (V_{SM}) capacitor and the V_{dc} voltage is as (8).

$$V_{dc} = NV_{SM}. \tag{8}$$

The step voltage on each branch is V_{SM}; from (7), we can calculate the number of SMs inserted as (9).

$$\begin{cases} N_U = \dfrac{v_U^{ref}}{V_{SM}} = \dfrac{V_{dc}}{2V_{SM}}\left(1 - m\cos\omega t\right) = \dfrac{N}{2}\left(1 - m\cos\omega t\right) \\ N_L = \dfrac{v_L^{ref}}{V_{SM}} = \dfrac{V_{dc}}{2V_{SM}}\left(1 + m\cos\omega t\right) = \dfrac{N}{2}\left(1 + m\cos\omega t\right) \end{cases}, \tag{9}$$

$$\begin{cases} N_U = \text{round}_{0.25}\left(\dfrac{u_U^{ref}}{U_d}\right) = \text{round}_{0.25}\left[\dfrac{V_{dc}}{2U_d}\left(1 - m\cos\omega t\right)\right] \\ N_L = \text{round}_{0.25}\left(\dfrac{u_L^{ref}}{U_d}\right) = \text{round}_{0.25}\left[\dfrac{V_{dc}}{2U_d}\left(1 + m\cos\omega t\right)\right] \end{cases}. \tag{10}$$

Figure 11(a) shows the upper and lower branch voltage, and the MMC phase voltage, and Fig. 11(b) shows the algorithm flowchart for NLM for the MMC. After the controller calculates the
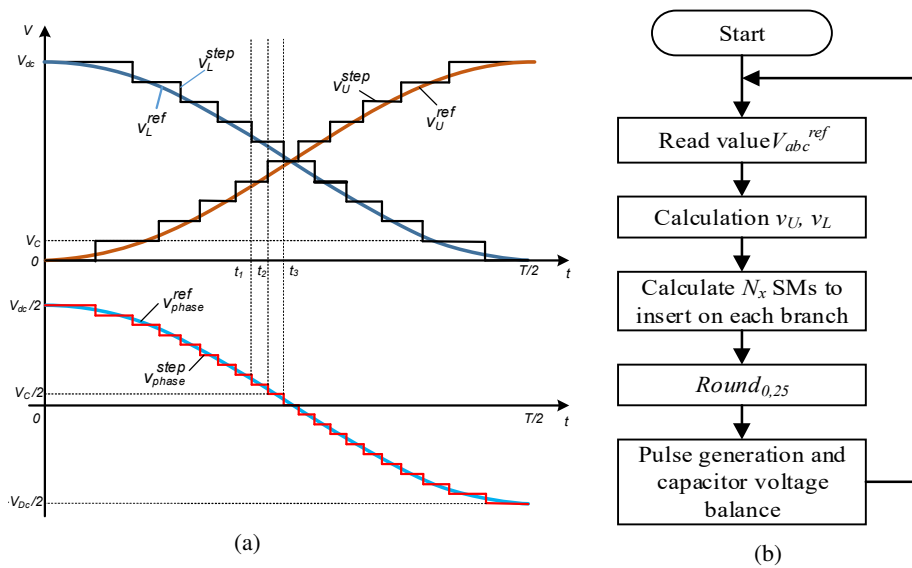

Fig. 11. Upper and lower branch voltage and MMC phase voltage (a);
flowchart of the algorithm for performing NLM (b)

reference value for the MMC voltage, the amount set for each phase's upper and lower branches is calculated based on the Formula (7). Then, the NLM method calculates the N_x SMs that must be inserted in the two branches of each phase through (9). The value of N_x is a positive integer, so after the calculation, the value of N_x needs to be rounded. In this paper, the rounding method of 0.25 (round 0.25) according to [12] is used, and from here, the number of SMs of the upper and lower branches at each time is calculated as (10).

3.3. Capacitor voltage balancing algorithm

We calculate the number of N_x of the SMs that need to be turned on using the NLM algorithm based on the input reference voltage value. The next problem to be solved is to select the number of N_x of the SMs that need to be turned on in a sampling cycle from the $2N$ SMs on each phase. To do this, we perform the capacitor voltage balancing algorithm, which means arranging the capacitor voltage values of the SMs, from which we select the N_x of the SMs that need to be turned on. At that time, the voltage of the capacitors that are turned on will have an oscillation value within an allowable range. This algorithm is shown explicitly in Fig. 12.
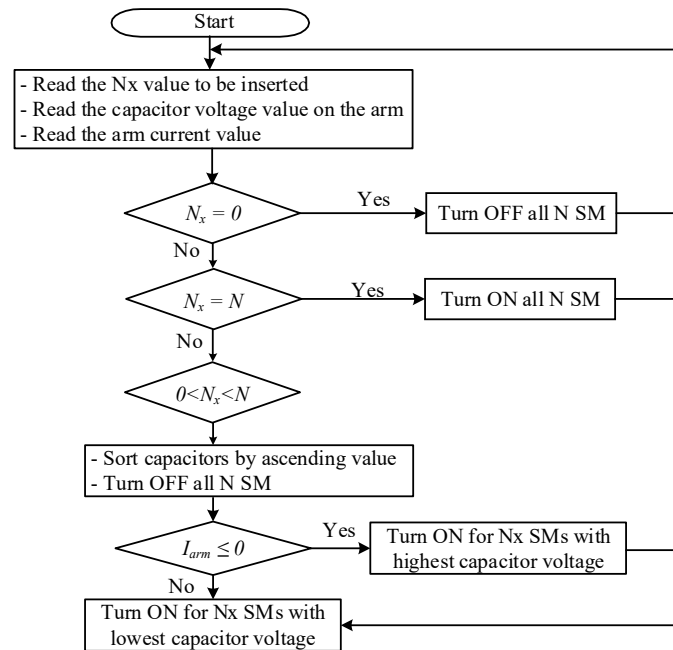

Fig. 12. Flowchart of capacitor voltage balancing algorithm

This method is simple to implement and does not require an additional capacitor voltage control loop. At the same time, these two methods cannot be separated. The NLM method will select the SMs to turn on during an MMC operating cycle, from which the new capacitor voltage balancing method has data to arrange the capacitor values to ensure that the capacitors are operated in a balanced state.

4. Design a control system, simulate and evaluate results

The structure of the control for the system is shown in Fig. 13. The structure consists of two control loops: the inner loop controls the current, and the outer loop controls the voltage. The current loop uses AC adjustment; the current value measured on the *abc* reference frame is then converted to the *dq* frame, compared with the reference value, the error is fed into the current controller, and the output of the current loop is the reference voltage of the voltage regulation loop. This value is fed to the NLM stage and the capacitor voltage balancing stage to select the SMs to be turned on and to send the switching pulses to the IGBT valves of the MMC inverter on each phase. In addition, the control structure is also equipped with a controller to determine the MPPT point for the DC/DC Boost Converter. The simulation process is performed on MATLAB/Simulink software for 2.5 s with the system parameters in Table 3.

Table 3. System simulation parameters

| STT	Solar System	Symbol	Value	Unit
1	Power	P_{PV}	100	kW
2	Maximum voltage	V_{MMP}	273.5	V
3	Maximum current	I_{MMP}	368.28	A
	MPPT – Boost Converter			
4	Inductor	L_{boost}	8.5e-4	H
5	Capacitor	C_{boost}	0.0045	C
6	Switching frequency	f_{boost}	2000	Hz
	MMC parameters			
7	Branch inductor	L_o	4.7e-5	H
8	SM capacitor	C_{SM}	0.02	F
9	Number of SM	N	10	
10	Branch resistance	R_o	6.76e-4	Ω
11	Primary transformer voltage	V_{pri}	260	V
12	Secondary transformer voltage	V_{sec}	25	kV
13	Transformer power	P_{BA}	100	kVA
14	Grid inductance	L_f	2.5e-4	H
15	Grid resistance	R_f	0.019	Ω
16	Grid power	P_{grid}	100	kW
17	Grid voltage	V_{grid}	25	kV
18	Grid frequency	f_{grid}	50	Hz
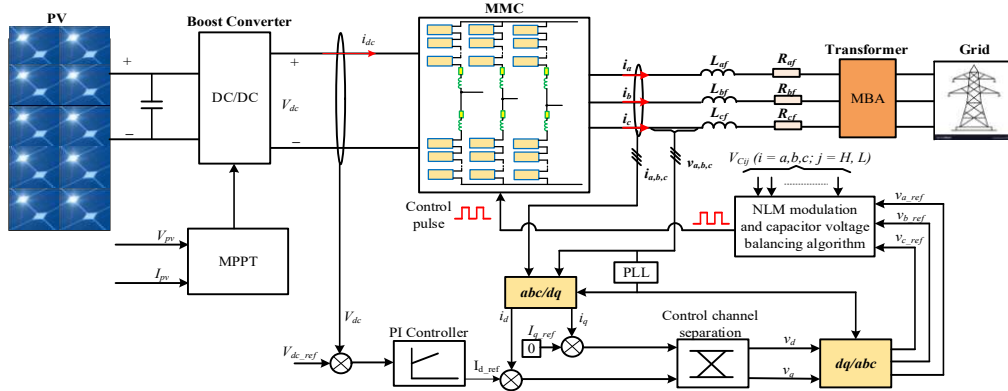
Fig. 13. Grid-connected PV–MMC system control structure

The scenario is simulated for the system with radiation intensity and temperature changes, as shown in Fig. 14(a). Initially, the intensity is 1000 W/m^2. After 0.6 s, the radiation decreases gradually to 250 W/m^2 within 0.5 s. At 1.2 s, the radiation gradually increases to 1000 W/m^2 within 0.5 s and remains the same until the end of 2.5 s. At time 2 s, the temperature rapidly rises to 50°C, checking the system response to the temperature change.
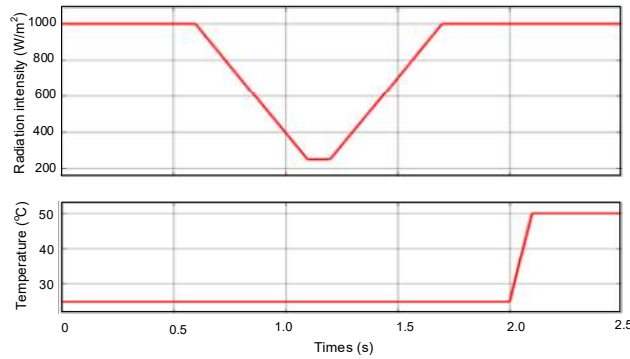
(a)
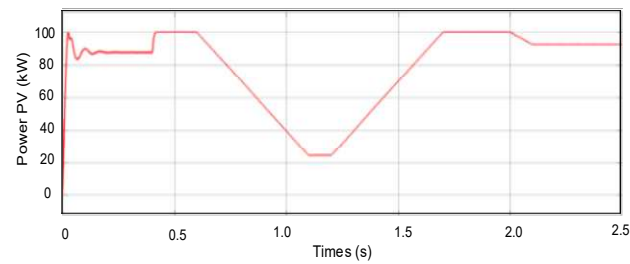
(b)

Fig. 14. Simulation of radiation intensity and temperature conditions (a); power of PV (b)

When simulating the system under the radiation conditions in Fig. 14(a), the power obtained after applying the MMPT algorithm is shown in Fig. 14(b). Initially, when MPPT is not turned on, the D coefficient is fixed at 0.55, and the PV power is stable at 86 kW. After 0.4 s, MPPT is turned on, and the PV power is adjusted to the maximum power (100 kW). From 0.6 s to 1.7 s, the solar radiation changes, the power also changes, and the simulation result is similar to the theory of radiation influence. At 2 s, the temperature increases to 50°C, leading to a decrease in the maximum power of the PV. The power graph is consistent with the original theory.

Figure 15 shows the change in operating voltage and current of the solar cell. Initially, the operating voltage and current are at 226 V and 384 A. After 0.4 s, the MPPT is turned on, and the voltage and current are adjusted to the maximum power point (V_{pv} = 273.5 V; I_{pv} = 368 A). The values of V_{pv}, and I_{pv} are consistent with the initial parameters in Table 1. When the solar radiation changes from 1000 W/m2 to 250 W/m2, the VMMP voltage of the cell decreases slightly to about 268 V; when the radiation returns to 1000 W/m2, the voltage increases again to 273.5 V; the operating current of the cell changes in the same form as the change in the intensity of I_r radiation. At time 2 s, the temperature increases to 50°C, causing the V_{MPP} voltage to decrease, the IMPP current to rise slightly, and the system works according to theory
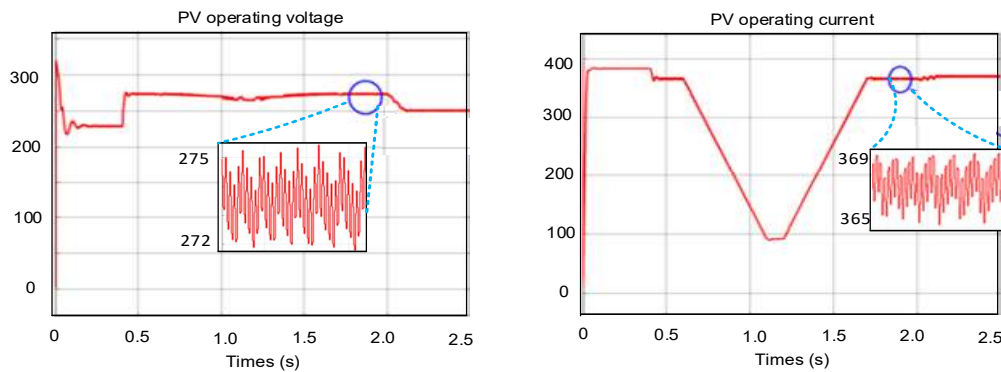

Fig. 15. Operating voltage and current of PV

The MPPT changes the modulation factor D of the Boost Converter. Initially, D is fixed at 0.55; after turning on the MPPT, the D cycle is adjusted. With the desired V_{dc} of 500 V, applying Formula (2), the ideal D value to be achieved is 0.45. Figure 16 shows the change of D through each stage, the first stage from 0 to 0.4 s (MPPT is not turned on), and D is kept fixed at 0.55. After turning on the MPPT, D is adjusted to fluctuate around the value of 0.45. The PV system is brought to operate at the maximum power point with fast speed and tiny deviation. During the period of 0.6–1.7 s, the radiation and V_{pv} voltage change, causing D to change accordingly. At 1.7 s, the radiation returns 1000 kW/m^2, and D is adjusted to the desired value. At 2 s, the temperature increases, causing the operating voltage of V_{pv} to decrease, and D rises to 0.504. Through the Boost Converter, the DC voltage is increased to 500 V. Figure 17 is the output V_{dc} voltage of the Boost Converter, which is also the V_{dc} value supplied to the MMC. The results show that the voltage response is excellent and close to the V_{dc-ref} set value of 500 V. The above results have demonstrated that the INC algorithm has given fast and accurate effects, which proves that the algorithm has met all the proposed MPPT goals for the PV system.
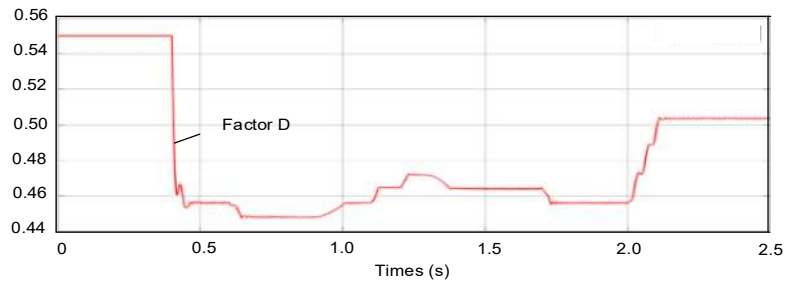
Fig. 16. Modulation factor *D* for Boost Converter
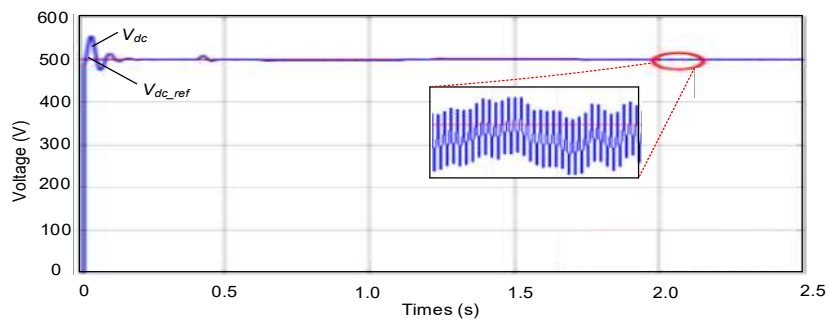
Fig. 17. DC side voltage of MMC

Figure 18 shows the MMC's current response I_d and I_q. Follow the reference value. The I_d graph is similar to the radiation; I_q is controlled to 0. The transient process only occurs in the first 0.1 seconds, which proves that the PI controller has given an excellent response.


(a)

(b)
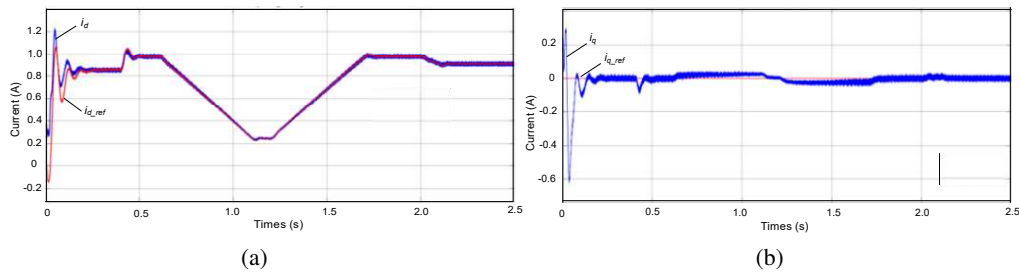
Fig. 18. Response of current *Id* vá *Iq*

Figure 19 shows the capacitor voltage on the MMC's SM. Thanks to the capacitor voltage balancing algorithm, the capacitor voltage is always kept stable at a rated value of 50 V. Its deviation is in the range of 44 V to 56 V, which is 12% and is a guaranteed and acceptable value for the MMC to operate stably for a long time.
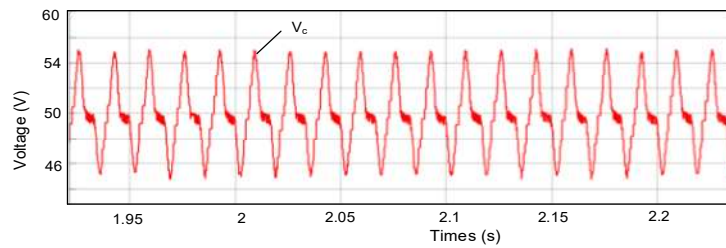
Fig. 19. Capacitor voltage of an SM when applying capacitor voltage balancing algorithm

Figure 20(a) and Fig. 21(a) show the MMC output voltage and current; the results show that the current and voltage are always sinusoidal. The MMC output voltage follows the set value and has a 21-level form, which is in accordance with the principle of NLM. The THD value of the output voltage is shown in Fig. 20(b), which is 3.32%; the THD value of the output current is shown in Fig. 21(b), which is 4.68%, and indicates that the output voltage and current are good quality.
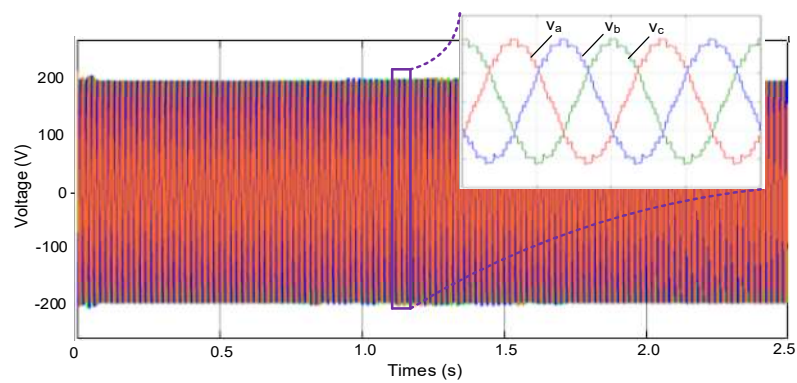

(a)
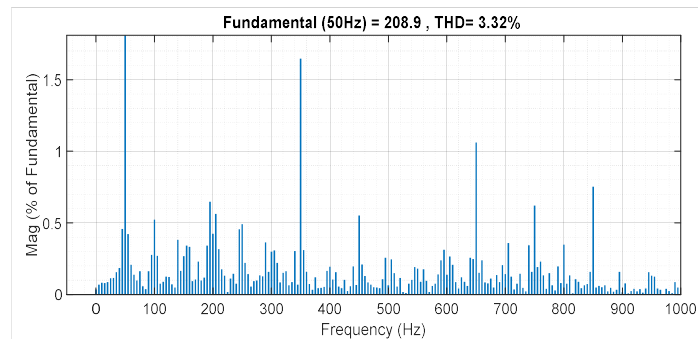
(b)

Fig. 20. Output voltage of the MMC and THD index of voltage

(a)

(b)
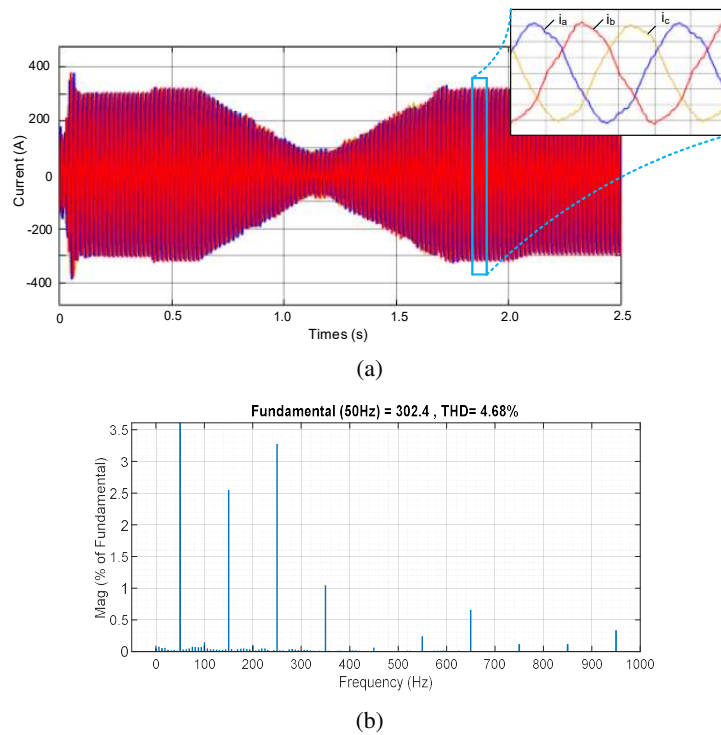
Fig. 21. Output current of the MMC and THD index of current

The DC voltage, after passing through the MMC, becomes AC voltage and is fed into the transformer to increase the voltage to the grid with a peak amplitude equal to a grid voltage amplitude of 20 kV; the current on the grid is small, about 3 A, shown in Figs. 22(a) and 22(b), respectively.


(a)

(b)
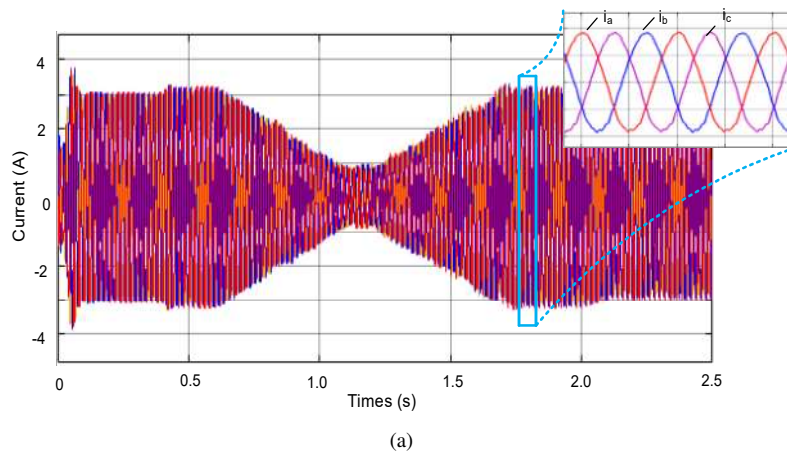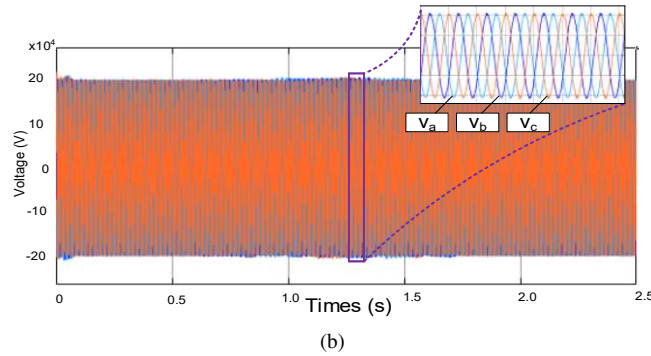
Fig. 22. Grid current (a); grid voltage (b)

Figure 23 shows the output power of the PV–MMC system. Under standard conditions, the maximum power achieved is about 95.5 kW, close to the required reference value. The difference is 4.5 kW, corresponding to 4.5%. This shows that the solar panel system has achieved an efficiency of 95.5%. This is a good value to absorb the maximum power from the solar power system.
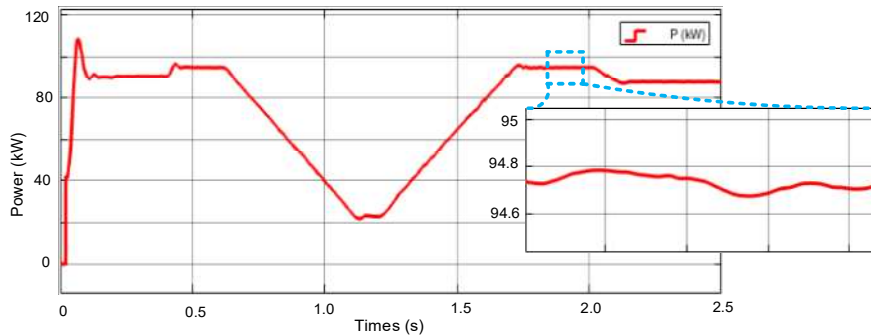

Fig. 23. Output power of PV–MMC system to the grid

5. Conclusion

This paper presents the structure of the grid-connected PV system through two converters: a Boost Converter and MMC. The implementation process has analysed the operation of the PV system and the factors affecting the energy conversion process. At the same time, the operation and the principle of MPPT point control for Boost Converter, control of the grid-connected MMC operation through NLM algorithm, capacitor voltage balancing algorithm and grid-connected PI control for MMC have also been analysed. The results show that the MPPT tracking performance of the PV system is good, specifically: when the set power requirement changes from 86 kW to 100 kW with changing temperature and radiation conditions, the algorithm only takes about 0.4 seconds to achieve the maximum power response close to a set value of 95.5 kW. This algorithm also takes only 0.4 seconds to achieve the desired current and voltage values corresponding to the required maximum power. The current results show that the Boost Converter's output DC

and voltage closely follow the set value with acceptable small fluctuations. The output AC and voltage of the MMC are sinusoidal with low THD indexes of 3.32% and 4.68%, respectively, which are low values within the acceptable range. The voltage value on the capacitor of the MMC is controlled to fluctuate around the equilibrium position with a low deviation of 12%, which is acceptable for the capacitor to operate stably in the long term. The above results of the paper have demonstrated that the INC algorithm combined with MPPT, PI control combined with NLM and the capacitor voltage value balancing algorithm have given excellent efficiency to the MMC and achieved all the set goals. This is the basis for applying the power circuit system and control circuit to large-capacity PV systems described in this paper.

References

[1] Lakshmanan S.A., Bharat S.R., Devanathan B., Oorappan G.M., *Modelling and Analysis of Tri-State Boost Converter for Solar PV Applications*, 2023 3rd International Conference on Emerging Frontiers in Electrical and Electronic Technologies (ICEFEET) (2023), DOI: 10.1109/ICEFEET59656.2023.10452243.

[2] Yahya A., Fadil E., Oulcaid H., Ammeh M., Giri L., *Guerrero, Control of grid connected photovoltaic systems with microinverters: New Theoretical design and numerical evaluation*, Asian J. Control, vol. 21, no. 1, pp. 1–13 (2017), DOI: 10.1002/asjc.1704.

[3] Shukla K., Sudhakar K., Baredar P., Mamat R., *Solar PV and BIPV system: Barrier challenges and policy recommendation in India*, Renewable and Sustainable Energy Reviews, vol. 82, pp. 3314–3322 (2018), DOI: 10.1016/j.rser.2017.10.013.

[4] Aziz S., Tajuddin M., Zidane T., Alwazzan M., *Design and optimization of a grid-connected solar energy system: Study in Iraq*, Sustainability, vol. 14, no. 13, 8121 (2022), DOI: 10.3390/su14138121.

[5] Taha A., Babiker S., *Design and Simulation of Voltage Source Grid Connected Inverter (VSI)*, 2018 International Conference on Computer, Control, Electrical, and Electronics Engineering (2018), DOI: 10.1109/ICCCEEE.2018.8515850.

[6] Ganyao W., Jing L., Chuanwei L., Han W., Yu Y., *Stability Analysis of Grid-Connected Wind Power Systems Based on SiC Devices*, 2024 IEEE 10th Intern. Power Electronic and Motion Control Confer. (IPEMC2024-ECCE Asia) (2024), DOI: 10.1109/IPEMC-ECCEAsia60879.2024.10567641.

[7] Logeswaran T., Monika N., Karuppusamy P., Vinosh M., Uthirasamy R., Raghavendran P.S., *Implementation and Analysis of Hybrid Solar PV and Wind Energy based Microgrid*, 2022 International Conference on Edge Computing and Applications (ICECAA) (2022), DOI: 10.1109/ICECAA55415.2022.9936214.

[8] Wang K., Lixun Z., Weimin W., Youngjong K., Rongwu Z., *Cascaded H-bridge Converter-based Large-Scale Photovoltaic Systems : Power Imbalance and Topology Derivation*, 2021 IEEE 12th Energy Conversion Congress & Exposition – Asia (2021), DOI: 10.1109/ECCE-Asia49820.2021.9479315.

[9] Dekka A., Wu B., Perez M., Zargari R., *Evolution of topologies modeling control schemes and applications of modular multilevel converters*, IEEE Journal of Emerging and Selected Topics in Power Electronics, vol. 5, no. 4, pp. 1631–1656 (2017), DOI: 10.1109/JESTPE.2017.2742938.

[10] Jiang Z., Beniwal N., Ceballos S., Pou J., Farivar G., *Analysis of the Average Neutral-Point Current Limits of the Neutral-Point-Clamped Converter Under Three-Level Modulation*, IECON 2020 The 46th Annual Conference of the IEEE Industrial Electronics Society, pp. 4079–4084 (2020), DOI: 10.1109/IECON43393.2020.9255382.

[11] Sakamoto M., Haga H., *Control Method for Single-Phase Active Filter Using Universal Smart Power Module*, International Power Electronics Conference 2022(IPEC 2022), pp. 1288–1293 (2022) DOI: 10.1541/ieejjia.22006895.

[12] Wang Y., Wu Y., Cui Y., Xu N., Wang P., Cao H., *Harmonics analysis and simulation of NLM in MMC*, 2016 China International Conference on Electricity Distribution (2016), DOI: 10.1109/CI-CED.2016.7575958.

[13] Fujin D., Qian H., Chengkai L., Yongqing L., Qingsong W., Dan Liu., *Circulating current suppression for MMC-HVDC systems with asymmetric arm impedance*, CSEE Journal of Power and Energy Systems, vol. 7, iss., pp. 530–540 (2021), DOI: 10.17775/CSEEJPES.2019.02690.

[14] Alamsyah A., Andarini A., Zulfiana S.M., *DC-DC converter using maximum power point tracker (MPPT) perturb and observe (P&O) algorithm in large-scale PV system*, vol. 3140, iss. 1, pp. 450–457 (2024), DOI: 10.1063/5.0221463.

[15] Hsu T., Wu H., Tsai D., *Photovoltaic Energy Harvester with Fractional Open-Circuit Voltage Based Maximum Power Point Tracking Circuit*, IEEE Transactions on Circuits and Systems II: Express Briefs, vol. 66, no. 2, pp. 257–261 (2019), DOI: 10.1109/TCSII.2018.2838672.

[16] Sohel S., Alice C., *Modelling and Simulation of Maximum Power Point Tracking Algorithm based PV Array and Utility Grid Interconnected System*, 2018 International Conference on Recent Innovations in Electrical, Electronics & Communication Engineering (2020), DOI: 10.1109/ICRIEECE44171.2018.9009106.

[17] Razman A., *Design of boost converter based on maximum power point resistance for photovoltaic applications*, 2015 International Conference on Renewable Energy Research and Applications ICRERA 2015, pp. 1580–1585 (2015), DOI: 10.1016/j.solener.2017.12.016.

[18] Nademi H., Das A., Burgos R., Norum E., *A New Circuit Performance of Modular Multilevel Inverter Suitable for Photovoltaic Conversion Plants*, IEEE Journal of Emerging and Selected Topics in Power Electronics, vol. 4, no. 2, pp. 393–404 (2016), DOI: 10.1109/JESTPE.2015.2509599.

[19] Yumeng Tian, Harith R. Wickramasinghe, Zixin Li, Georgios Konstantinou, *Modular Multilevel Converter Sub-modules for HVDC Applications*, 2020 IEEE 9th International Power Electronics and Motion Control Conference (IPEMC2020-ECCE Asia), 09 March 2021, DOI: 10.1109/IPEMC-ECCEAsia48364.2020.9368019.

[20] Mana S., Hitoshi H., *Three-Phase Modular Multilevel Converters Composed of Universal Smart Power Module*, 2022 IEEE Energy Conversion Congress and Exposition (ECCE) (2022), DOI: 10.1109/ECCE50734.2022.9948053.

[21] Wang K., Lixun Z., Weimin W., Youngjong K., Rongwu Z., *Cascaded H-bridge Converter-based Large-Scale Photovoltaic Systems: Power Imbalance and Topology Derivation*, 2021 IEEE 12th Energy Conversion Congress & Exposition – Asia (2021), DOI: 10.1109/ECCE-Asia49820.2021.9479315.